Modeling of apparent radar reflectivity due to convective clouds at attenuating wavelengths

Frank S. Marzano

Dipartimento di Ingegneria Elettrica, Centro di Eccellenza CETEMPS, Università dell'Aquila, L'Aquila, Italy

Laura Roberti[1]

BTexact Technologies, Ipswich, UK

Sabatino Di Michele, Alberto Mugnai, and Alessandra Tassa

Istituto di Scienze dell'Atmosfera e del Clima (ISAO), Consiglio Nazionale delle Ricerche (CNR), Rome, Italy

Received 13 February 2002; revised 29 May 2002; accepted 18 September 2002; published 4 January 2003.

[1] Spaceborne precipitation radars are usually designed to operate at attenuating wavelengths, mostly at X, Ku and Ka band. At these frequencies and above, convective rainfall can cause severe attenuation. Moreover, raindrops and precipitating ice can give rise to appreciable multiple scattered radiation which apparently tends to enhance the nominal attenuated reflectivity. In order to properly describe radar observations in such conditions, apparent reflectivity has to be modeled taking into account both path attenuation and incoherent effects. To this aim, a general definition of volume radar reflectivity is introduced, and a Monte Carlo model of backscattered specific intensity is implemented. The numerical model is applied to synthetic profiles, extracted from a mesoscale cloud-resolving model simulation and representing intense and heavy convective precipitation at a developing and mature stage. Realistic appearance of these average profiles is argued by resorting to radar measurements available in literature. Spaceborne apparent reflectivity due to multiple scattering is shown to be significantly different from the attenuated one for the near-surface layers of mature convection at Ku band and even for growing convection at Ka band. A discussion about this discrepancy is carried out at Ku band showing its possible impact for estimated rain rate profiles. If precipitation incoherent effects are formally treated as perturbation factors of the specific attenuation model, constrained single-frequency inversion techniques are shown to be suitable to minimize rain rate retrieval errors due to multiple scattering phenomenon. *INDEX TERMS:* 6952 Radio Science: Radar atmospheric physics; 3359 Meteorology and Atmospheric Dynamics: Radiative processes; 0689 Electromagnetics: Wave propagation (4275); 3354 Meteorology and Atmospheric Dynamics: Precipitation (1854); *KEYWORDS:* rainfall, microwave radar, attenuating wavelength, radiative transfer, path attenuation, Monte Carlo technique

Citation: Marzano, F. S., L. Roberti, S. Di Michele, A. Mugnai, and A. Tassa, Modeling of apparent radar reflectivity due to convective clouds at attenuating wavelengths, *Radio Sci.*, *38*(1), 1002, doi:10.1029/2002RS002613, 2003.

1. Introduction

[2] Spaceborne and airborne radar sensing and profiling of precipitation has been well established in the last two decades [*Meneghini*, 1978; *Fujita*, 1983; *Marzoug and Amayenc*, 1991; *Haddad et al.*, 1996]. This research and development activity has culminated with the launch of the Tropical Rainfall Measuring Mission (TRMM) platform on November, 1997 [*Kummerow et al.*, 1998]. Aboard the TRMM platform, data acquired by the Precipitation Radar (PR) represent a unique opportunity to verify the expectations on the accuracy of rain retrievals from space in the tropical region [*Iguchi et al.*, 2000]. Indeed, various airborne campaigns were also

[1]Formerly at Dipartimento di Elettronica, Politecnico di Torino, Torino, Italy.

0048-6604/03/2002RS002613$11.00

carried out as preparatory and validation experiments, using TRMM-prototype sensors [*Kumagai and Meneghini*, 1993; *Marzano et al.*, 1994; *Marecal et al.*, 1997]. Their high spatial resolution data have been widely utilized to understand the potential and limitation of spaceborne sensor capabilities.

[3] Several rain retrieval techniques have been developed so far using space-based radar reflectivity measurements [*Iguchi and Meneghini*, 1994; *Marzoug and Amayenc*, 1994]. The use of radar reflectivity measurements between 10 and 35 GHz has been investigated to estimate precipitation profiles from single-frequency, dual-frequency and dual-beam observations [*Meneghini et al.*, 1989; *Testud et al.*, 1992]. The formulation of these estimation methods basically relies on the solution of the radar equation in an attenuating medium in either a deterministic or stochastic form. Further constraints, derived from radiometric measurements or from surface-reference radar techniques, are generally added in the inverse problem in order to ensure the stability of the solution itself [*Weinman et al.*, 1990; *Marzano et al.*, 1999a; *Marzano and Bauer*, 2001].

[4] The radar equation in an attenuating medium, as generally stated, takes into account the single scattering due to raindrops weighted by the path attenuation from the considered range gate to the radar antenna. However, for frequencies higher than 10 GHz and for intense-to-heavy convective rainfall, the albedo and the scattering asymmetry factor of raindrops and precipitating ice can be significant [*Smith et al.*, 1992; *Yeh et al.*, 1995; *Olson et al.*, 1996]. Under these conditions, the contribution of this incoherently scattered radiation can be appreciable in determining the radar received power [*Ishimaru et al.*, 1982; *Ito et al.*, 1995; *Oguchi et al.*, 1998]. Disregarding multiple scattering effects in the formulation of the radar forward problem could affect the accuracy of both the ranging and estimate of rainfall rate profile [*Oguchi et al.*, 1994; *Marzano et al.*, 2000].

[5] The objective of this work is to evaluate the possible impact of multiple scattering due to rainfall and ice graupel upon the radar response at Ku and Ka bands (i.e., 10- to 40- GHz) through a numerical investigation. The concept of radar apparent reflectivity is introduced in a general context and a backward Monte Carlo model is described to compute the received specific intensity. The effects of precipitation multiple scattering are evaluated at 14 and 35 GHz and for nadir observations. Realistic precipitation profiles are extracted from the outputs of a three-dimensional microphysical mesoscale cloud model and characterized through single-scattering optical parameters. Numerical results are shown and discussed in terms of the observed apparent reflectivity and of the derived rain rates from 13.8-GHz data for tropical convective profiles representing intense and heavy precipitation. Retrieval techniques, based on the inversion of the classical radar equation, are also analyzed in order to frame this incoherent echo effect as a possible error source removable by constraints such as the estimated total path attenuation.

2. Apparent Radar Reflectivity

[6] The classical radar equation is derived under the assumption of single-scattering conditions and can include path attenuation. However, when multiple scattering effects become relevant in an attenuating media, the mean apparent received power $\langle P_{Ra}(r)\rangle$ due to the range gate at distance r is expected to be higher than that expected from classical radar equation. If $\langle I_{Ra}(r)\rangle$ is the mean value of the apparent received specific intensity (in W m^{-2} sr^{-1} Hz^{-1}) along the radar boresight, then the apparent back-scattered received power $\langle P_{Ra}(r)\rangle$ can be expressed as [*Ishimaru*, 1978; *Tsang et al.*, 1985]:

$$\langle P_{Ra}(r)\rangle \equiv \int_{4\pi} A_e(\Omega')\langle I_{Ra}(r,\Omega')\rangle d\Omega' \qquad (1)$$

with $A_e(\Omega) = A_{eo}\,|f_n(\Omega)|^2$, where $A_{eo} = A_e(\Omega_o)$ is the maximum antenna equivalent area along the pointing angle of the radar antenna Ω_o, and $f_n(\Omega)$ is the normalized antenna field pattern function. Polarization properties of the received backscattered power are here disregarded [*Bringi and Hendry*, 1990; *Ito et al.*, 1995].

2.1. General Definition

[7] Let us define in a multiple scattering medium the volumetric apparent radar reflectivity η_a at a range r and in the direction Ω in a way analogous to the surface scattering coefficient σ^0 [*Tsang et al.*, 1985]. The latter can be generalized as follows [*Marzano et al.*, 2000]:

$$\eta_a(r,\Omega) >\equiv \frac{4\pi}{\Delta r}\frac{\langle I_{Ra}(r,\Omega)\rangle}{F_T(r,\Omega)} \qquad (2)$$

where $\Delta r = c\Delta t/2$ is the range resolution with Δt the pulse width and c the light velocity (in the medium) and F_T is the transmitted power flux density (in W m^{-2} Hz^{-1}) or Poynting's vector amplitude. The previous equation basically expresses the apparent reflectivity as a radar scattering cross-section per unit volume.

[8] In order to extend the classical radar equation, we need to explicitly express the transmitted power P_T. In the far-field zone the latter can be related to the transmitted power through

$$F_T(r,\Omega) >= \frac{G(\Omega)}{4\pi}\frac{P_T}{r^2} \qquad (3)$$

where $G(\Omega)$ is the antenna gain such that $G(\Omega) = G_0\,|f_n(\Omega)|^2$ with $G_0 = G(\Omega_0)$ the maximum (directive) gain.

The directive gain is related to the maximum antenna equivalent area A_{eo} through the reciprocity formula, that is $G_0 = 4\pi(A_{e0}/\lambda^2)$.

[9] Thus, substituting (2) and (3) in (1), we have

$$\langle P_{Ra}(r)\rangle = \frac{\Delta r}{4\pi}\int_{4\pi} A_e(\Omega')\eta_a(r,\Omega')\frac{G(\Omega')}{4\pi}\frac{P_T}{r^2}d\Omega' \quad (4)$$

[10] If $\langle I_{Ra}(r, \Omega)\rangle$, and thus $\eta_a(r, \Omega)$, can be assumed constant within the antenna main lobe (i.e., disregarding secondary lobes contribution), it is straightforward to reexpress the mean apparent received power as follows:

$$\langle P_{Ra}(r)\rangle \cong \left[\frac{G_0 A_{e0}\Omega_{2A}\Delta r}{(4\pi)^2}\right]\frac{P_T}{r^2}\eta_a(r,\Omega_0) \quad (5)$$

where Ω_{2A} is the two-way main-lobe solid angle, given by

$$\Omega_{2A} = \int_{\Omega_M} |f_n(\Omega')|^4 d\Omega' \quad (6)$$

with Ω_M the main-lobe angular width.

[11] The apparent radar reflectivity (in $mm^6\ m^{-3}$) can be expressed in the Ω_0 direction through the apparent reflectivity factor Z_a [*Sauvageot*, 1992]:

$$Z_a(\Omega_0, r) \equiv \frac{\lambda^4}{\pi^5|K|^2}\eta_a(\Omega_0, r) = \frac{\lambda^4}{\pi^5|K|^2}\frac{4\pi}{\Delta r}\frac{\langle I_{Ra}(\Omega_0, r)\rangle}{F_T(\Omega_0, r)} \quad (7)$$

where λ is the radar wavelength and K is the medium complex polarizability (equal to 0.93 for water drops). By substituting (7) in (5), we obtain a generalized radar equation which resembles the classical radar equation; that is,

$$\langle P_{Ra}(r)\rangle \cong C\frac{P_T}{r^2}Z_a(r,\Omega_0) \quad (8)$$

where the radar constant C is given by

$$C = \frac{G_0 A_{e0}\Omega_{2A}\Delta r\pi^3|K|^2}{16\lambda^4} \quad (9)$$

Notice that the receiver losses were neglected and the resulting equation is valid under the assumption of a uniform distribution of the random scatterers within the main beam (i.e., neglecting the nonuniform beam filling of the range volume). If the antenna power pattern is assumed to be Gaussian, the expression of the two-way main lobe solid angle in (6) yields the Probert-Jones correction factor to the radar equation given by (8) [*Sauvageot*, 1992].

[12] The generalized radar equation can be simplified when considering only single scattering phenomena by introducing the single scattering apparent reflectivity factor Z_{aSS}. We can define Z_{aSS} as

$$Z_{aSS}(r,\Omega_0) \equiv \frac{\lambda^4}{\pi^5|K|^2}\frac{4\pi}{\Delta r}\frac{\langle I_{Ra}(r,\Omega_0)\rangle_{SS}}{F_T(r,\Omega_0)} \quad (10)$$

where $\langle I_{Ra}(r, \Omega_0)\rangle_{SS}$ is the received specific intensity in the first-order scattering approximation. From the radiative transfer theory (see next section), it can be easily demonstrated that [*Ishimaru*, 1978; *Tsang et al.*, 1985]

$$Z_{aSS}(r,\Omega_0) = Z_e(r,\Omega_0)L^2(r) \quad (11)$$

where $Z_e(r, \Omega_0)$ is the equivalent reflectivity factor, computed at range r along the pointing direction Ω_0. The one-way attenuation factor, indicated by $L(r)$ (for brevity, we omit the Ω_0 dependence), is given by

$$L(r) = e^{-\int_0^r k(r')dr'} = e^{-\tau(r)} = e^{-A(r)/4.343} \quad (12)$$

where k is the volumetric extinction coefficient (or specific attenuation, in m^{-1}) of the considered range-gated scattering volume and τ is the optical thickness such that the one-way path attenuation (in dB) is $A = 4.343\ \tau$.

[13] By inserting $Z_{aSS}(r, \Omega_0)$ in (8), we reobtain the classical radar equation for $\langle P_{Ra}(r)\rangle_{SS}$:

$$\langle P_{Ra}(r)\rangle_{SS} \cong C\frac{P_T}{r^2}Z_e(r,\Omega_0)L^2(r) \quad (13)$$

which holds only if single-scattering hypotheses can be assumed for the considered frequency in a moderately attenuating medium. It is worth mentioning that, from both (8) and (13), the mean received power $\langle P_{Ra}(r)\rangle$ is proportionally dependent on Ω_{2A} through C under the assumption of uniform beam filling, while $Z_a(r,\Omega_0)$ is by definition normalized with respect to Ω_{2A}.

2.2. Monte Carlo Model of Specific Intensity

[14] In order to evaluate radar reflectivity $Z_a(r, \Omega_0)$ from (7) and (10), the mean received specific intensity $\langle I_{Ra}(r,\Omega_0)\rangle$ must be computed as a function of the range r taking into account multiple scattering effects in an attenuating medium. Classical radar theory is not suitable to this purpose which can be tackled in an effective way by resorting to the radiative transfer modeling [*Ishimaru*, 1978; *Tsang et al.*, 1985; *Gasiewskii*, 1993]. The integro-differential equation which governs the scattered specific intensity $I(s, \Omega)$ can be stated as

$$\frac{dI(s,\Omega)}{ds} = -kI(s,\Omega) + \frac{k_s}{4\pi}\int_{4\pi} p(\Omega,\Omega')I(s,\Omega')d\Omega' + \frac{k_s}{4\pi}p(\Omega,\Omega_0)F_T(\Omega_0)e^{-\tau} \quad (14)$$

where s is the distance coordinate, k_s is the volumetric scattering coefficient (such that $k = k_a + k_s$ with k_a the volumetric absorption coefficient) and $p(\Omega_s) = p(\Omega,\Omega')$ is the volumetric scattering phase function with Ω_s the scattering solid angle (normalized to 1 over 4π). Note that (14) holds in case of an incident collimated beam of flux density F_T at the medium boundary and, if the medium is inhomogeneous, volumetric coefficients themselves depend on s.

[15] Multiple scattering effects are described by the second term of the right-hand side of (14), depending on the scattering coefficient and phase function efficiency. Range volume bins characterized by large scattering phenomena, that is high albedo (defined as $w = k_s/k$) and large asymmetry factors g (equal to 2/3 of the first moment of p expanded in Legendre polynomials), are expected to significantly contribute to multiple scattering. Precipitating ice particles typically present these features (see section 3.1) [*Gasiewskii*, 1993; *Marzano et al.*, 2000].

[16] Several numerical techniques are currently available to solve (14) under given boundary conditions and medium geometry [*Tsang et al.*, 1985]. In this work a backward one-dimensional (1-D) Monte Carlo method, making use of a biasing technique in order to reduce the computational time, was developed in order to simulate radar observations [*Roberti*, 1997]. Even if the adopted Monte Carlo method has 3-D capabilities, a 1-D framework was adopted in order to focus on the multiple scattering effects, thus avoiding modeling complications [*Roberti et al.*, 1994; *Marzano et al.*, 1999b]. The choice of a Monte Carlo solution was also suggested by the strict analogy between the algorithm flow chart and the radar observation mechanism [*Lin and Sarabandi*, 1999].

[17] A plane-parallel atmosphere was considered, characterizing each layer through hydrometeor contents and relative optical parameters (that is, k, w and p). Assuming a uniform vertical resolution, a number N_L of cloud layers was considered. The adopted observation geometry is referred, for simplicity, to an airborne nadir-looking radar as shown in Figure 1. The source beam is represented by a collimated flux density, incident on the top boundary from nadir so that $\Omega_0 = (\theta_0,\varphi_0) = (0,0)$ with θ_0 and φ_0 the incident zenith and azimuth angles. In this case, range direction coincides with altitude and each layer can be ideally associated to a range bin.

[18] A biasing technique is used in order to prevent the photons from escaping the medium and to enhance algorithm efficiency [*Roberti*, 1997]. The procedure is initiated by releasing a microwave photon from the point where the received intensity has to be computed, i.e. at the radar antenna in the receiving mode, with a direction opposite to the one it would physically propagate, i.e. going downward to the radar antenna in the transmitting mode. A unitary weight W is assigned to each released photon associated to a flux density F_T.

[19] The optical distance to the collision τ_c is computed from

$$\rho = e^{-\tau_c} \tag{15}$$

where ρ is a random number uniformly distributed between 0 and 1. If the photon crosses a layer (range bin) boundary, it is advanced to the boundary itself and a new τ_c is computed, taking memory of the distance already traveled. If a collision occurs in a given range bin (i.e., $w > 0$), then a scattering is forced to happen in order to avoid absorption: the corresponding bias is removed by multiplying the photon weight W by the single scattering albedo w of the range bin itself. If τ_c is such that the photon path intersects the upper boundary corresponding to the radar antenna location, a collision is forced by selecting the optical distance from the truncated exponential distribution [*Collins et al.*, 1972]. The bias introduced by forcing the collision, is removed by properly reducing the photon weight [*Roberti*, 1997].

[20] The algorithm keeps track of the optical distance traveled by each photon. When the first scattering occurs in the volume bin at range r, the algorithm computes the contribution to the received intensity given by the first scattering of the radar radiation by the n-th photon as

$$I^1_{Ra_n}(r,\Omega_0) = F_T W^1_n p\left(r,\Omega^1_{R_n}\right) e^{-\tau^1_n(r)} \tag{16}$$

where W_n^1 is the weight attached to the n-th photon after the first scattering event and equal to the range-bin albedo w, τ_n^1 is the optical depth (see Figure 1) measured from the photon position where the scattering occurs in the considered the range bin to the radar antenna in the direction antiparallel to the pointing direction Ω_0, (i.e. $-\Omega_0$). The term $p(r, \Omega^1_{Rn})$ is the scattering phase function evaluated at Ω^1_{Rn}, where Ω^1_{Rn} is the angle between the photon incident direction and $-\Omega_0$. Clearly, for single back-scattering it holds: $\Omega^1_{Rn} = \pi$. In order to identify the range bin, the total length traveled by the photon, before the scattering, is added to the path length from the current photon position to the top of the atmosphere in the radar pointing direction Ω_0. Dealing with two-way paths, this total length, divided by two and called r, is then compared with the bin ranges r_j with $j = 1$ to $N_L + 1$. If $r_{j-1} < r < r_j$, then the received intensity (16) can be associated to j-th bin.

[21] When multiple scattering is present, the previous association may be physically ambiguous [*Marzano et al.*, 2000]. The n-th photon can experience more than one scattering event and travel in any direction (not necessarily in the radar pointing one). In correspondence to the i-th scattering event of the n-th photon, the received

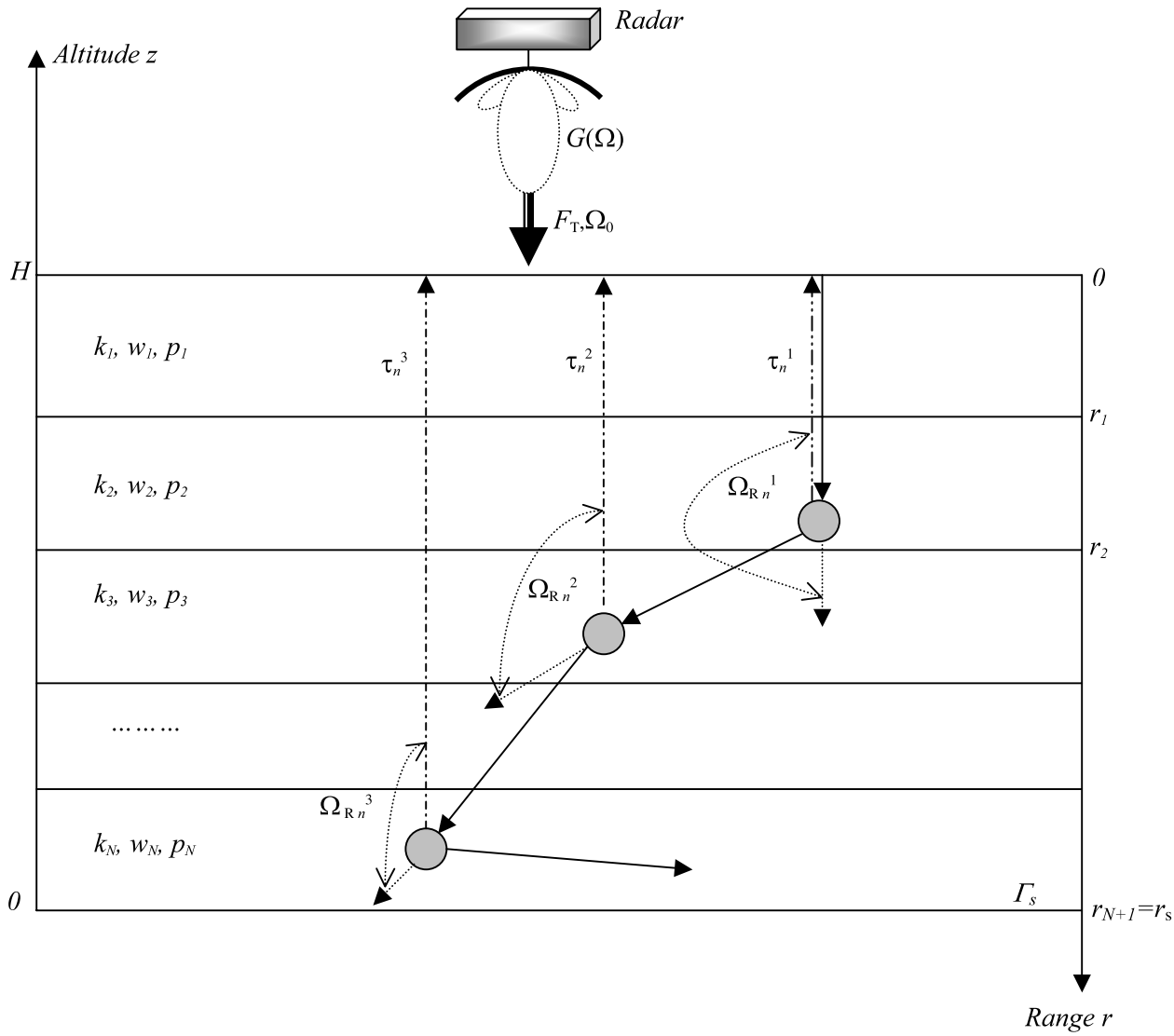

Figure 1. Geometry and principles of backward Monte Carlo algorithm to compute the received apparent specific intensity $I_{Ra}(r,\Omega_0)$ at a range r due to the n-th photon in the pointing direction Ω_0, chosen as nadir in the figure. Only a process of third-order scattering is represented for simplicity. The atmosphere is subdivided into N_L layers (range bins) characterized by extinction coefficient k, albedo w and phase function p. The radar source is described through its directive gain G and flux density F_T, while the Lambertian surface at range $r = r_s$ (altitude $z = 0$) is denoted by its albedo Γ_s. Solid lines refer to the optical distance to collision τ_c (backward from the radar receiver), while other symbols are illustrated in equations (16) and (17).

apparent specific intensity I_{Ra} from a given bin at range r can be assigned by generalizing (16) as

$$I^i_{Ra_n}(r,\Omega_0) = F_T W^i_n p\left(r,\Omega^i_{R_n}\right) e^{-\tau^i_n(r)} \qquad (17)$$

where W^i_n is the weight attached to the n-th photon after the i-th scattering event and $p(r,\Omega^i_{Rn})$ is the scattering phase function evaluated at the angle Ω^i_{Rn} between the photon incident direction and the direction opposite to the radar pointing direction (see Figure 1). The optical thickness τ^i_n in (17) is a generalization of τ^1_n to i-th scattering event. Equations (17) and (16) are strictly valid in case of a nonspecular lower surface, otherwise they should be modified to take into account an extra

contribution to the intensity due to the surface albedo Γ_s [*Roberti*, 1997].

[22] To a certain extent, the phase function $p(r, \Omega^i_{Rn})$ represents the probability that the n-th photon is scattered in the pointing (zenith) direction, while $exp(-\tau^i_n)$ indicates the probability that the n-th photon propagates from the considered range bin to the top of the atmosphere without undergoing any other collision. Notice that, following the procedure previously outlined, (17) is apparently attributed to j-th range bin since r takes into account the total path length due multiple scattering processes.

[23] The procedure is repeated until the photon weight becomes smaller than a given threshold, several orders of magnitude less than the intensity to be computed [*Morel and Gentili*, 1991]. After N_p photons have been released, the mean apparent intensity $\langle I_{Ra}(r, \Omega_0)\rangle$, received by the radar from a given range bin by taking into account the multiple scattering effects, is computed as

$$\langle I_{Ra}(r,\Omega_0)\rangle = \frac{1}{N_p}\sum_{n=1}^{N_p}\sum_{i=1}^{N_s} I^i_{Ra_n}\left(r,\Omega^i_{R_n}\right) \qquad (18)$$

where N_s is the number of scattering events of the n-th photon in the given volume bin at range r. The number N_p of released photons is chosen to ensure the algorithm convergence and a constant value of the product N_p by N_s within each layer (range bin) [*Morel and Gentili*, 1991; *Roberti*, 1997].

[24] As a particular case of (18), when considering only single scattering effects, the mean received intensity $\langle I_{Ra}(r,\Omega_0)\rangle_{SS}$ is computed by interrupting the process described above at the first order of scattering as in (16); that is, for $i = 1$,

$$\langle I_{Ra}(r,\Omega_0)\rangle_{SS} = \frac{1}{N_p}\sum_{n=1}^{N_p} I^1_{Ra_n}\left(r,\Omega^1_{R_n}\right) \qquad (19)$$

[25] From previous results and using (2), the apparent radar reflectivity along the pointing direction Ω_0 can be expressed as

$$\eta_a(r,\Omega_0) = \frac{4\pi}{\Delta r}\frac{1}{N_p}\sum_{n=1}^{N_p}\sum_{i=1}^{N_s} W^i_n p\left(r,\Omega^i_{R_n}\right)e^{-\tau^i_n(r)} \qquad (20)$$

which interestingly represents a new probabilistic definition of η_a itself. Finally, from (7) and (8), the apparent received mean intensity $\langle I_{Ra}(r,\Omega_0)\rangle$ can be converted into mean apparent received power $\langle P_{Ra}(r)\rangle$ by

$$\langle P_{Ra}(r)\rangle \cong C\frac{P_T}{r^2}\frac{\lambda^4}{\pi^5|K|^2}\frac{4\pi}{\Delta r}\frac{1}{N_p}\sum_{n=1}^{N_p}\sum_{i=1}^{N_s} W^i_n p\left(r,\Omega^i_{R_n}\right)e^{-\tau^i_n(r)} \qquad (21)$$

where all terms were previously described.

3. Numerical Analysis

[26] In order to compute (20) and analyze numerical outputs, vertical profiles of precipitating clouds need to be simulated. *Ad hoc* simple structures, as rain slabs, might be employed to this aim [*Ishimaru et al.*, 1982; *Oguchi et al.*, 1994; *Ito et al.*, 1995]. Even though we used these examples to validate the Monte Carlo algorithm with results available in the literature, this choice reveals to be limited. As previously noted, ice hydrometeor layers with high albedo in cloud convection regions are expected to contribute most to incoherent multiple scattering. Moreover, hydrometeor vertical profiles both in liquid and ice phase are likely to be nonuniform. A way to approach the problem in a more realistic way is to resort to mesoscale cloud-resolving models with explicit hydrometeor microphysics [*Yeh et al.*, 1995; *Olson et al.*, 1996; *Marzano et al.*, 1999a, 1999b]. The advantage of this choice is to deal with vertical cloud structures with an inherent consistency of its microphysical processes. On the other hand, limitations of dynamical and microphysical assumptions of the cloud-resolving model will reflect on output vertical profiles themselves.

[27] Our analysis is focused on convective stages of precipitating clouds in order to emphasize the incoherent backscattering effects and to show the possible difference between attenuated and apparent reflectivity, given by (11) and (7) respectively. The numerical simulations are carried out for spaceborne radar observations at nadir with a range resolution of 500 m (corresponding to a pulse duration Δt of 3.3 μs) for the two frequency bands at 13.8 (hereinafter, also referred to as 14 GHz) and 35 GHz. The receiver is assumed to be able to process contiguous range bins.

[28] In the following sections we will briefly introduce the procedure followed to extract convective precipitation profiles, together with an overview of the optical parameter computations relevant to the radar equation in scattering media. Numerical results of simulated apparent reflectivity profiles will be discussed together with the possible impact of multiple scattering effects on inversion procedures.

3.1. Convective Rainfall Characterization

[29] The raining cloud profiles were obtained from the cloud microphysical-dynamical model developed by *Tao et al.* [1987]. The cloud domain consists in 64 × 64 pixels, available every 15 minutes during the evolution of the simulated storm. A single time-step, corresponding to 210 minute of the simulation and modeling the mature stage of a squall line over the Indian Ocean, was chosen in this study. The characteristics of the model outputs and its microwave appearance are also described by *Roberti et al.* [1994] and *Olson et al.* [1996]. Each pixel consists

of 28 vertical layers from the surface to a height of 18 km with a variable vertical resolution (from hundreds to thousands of meters). The 28 layers of the original cloud model were resampled to 36 layers having a 0.5-km thickness. This choice was made in order to have the layer thickness compatible with a typical range resolution of a spaceborne radar (e.g., PR has a 250-m range resolution).

[30] For each grid cell the cloud model specifies height, pressure, temperature, relative humidity, together with cloud water, rainwater, cloud ice, snow and graupel equivalent water contents (EWCs). Rain and graupel densities ρ were set, respectively, to 1 g cm^{-3} and 0.4 g cm^{-3}. All hydrometeors' shape was assumed to be spherical: even though this assumption is not always valid (especially for ice crystals), the related error was considered to be of second-order here. An inverse-exponential particle size distribution (PSD) with a variable logarithmic slope was used for snow, rain and graupel particles. The general PSD form is the following $N(D) = N_o \exp(-\Lambda D)$, with the "logarithmic slope' Λ of $ln[N(D)]$ given by $\Lambda = (\pi\rho N_o/L_h)^{0.25}$, being L_h the hydrometeor equivalent water content in g m^{-3} [*Marzano and Bauer*, 2001]. The "intercept' N_o of $ln[N(D)]$ is constant and equal to 0.08 cm^{-4} for rain, as in the Marshall-Palmer distribution, and to 0.04 cm^{-4} for snow and graupel. A modified Gamma distribution was adopted for cloud droplets, while the gaseous absorption was computed by means of the Liebe model [*Roberti et al.*, 1994].

[31] Since in this work our analysis was limited to plane-parallel atmospheric structures, a limited set of precipitation profiles were extracted from the cloud-model grid belonging to the convection area. In particular, 16 vertical columns (pixels) were selected in correspondence of 2 classes (with 8 samples each) with columnar precipitating-ice content around 10 kg/m^2 and 20 kg/m^2, respectively. The hydrometeor vertical profiles (and the attached meteorological variables) of each of these 2 classes were horizontally averaged. The result of this procedure was the generation of a set of 2 average profiles characterizing intense and heavy convective rainfall.

[32] Left panels of Figure 2 show the obtained average profiles of cloud (nonprecipitating liquid), rain (precipitating liquid), graupel (precipitating ice), and snow (nonprecipitating ice) equivalent water contents for the intense and heavy convective profiles. Note that the profile labeled "Heavy convective precipitation profile" is indeed similar to that labeled "Intense rainfall profile" by *Marzano et al.* [2000]. The synthetic convective profiles are characterized by a large amount of graupel and rain above and below the freezing level around 4.5 km, respectively. Heavy convection presents a structure similar to the intense one, but with much higher liquid and ice contents.

[33] Due to the sphericity assumption of the hydrometeors, the Mie theory was used for computing the optical parameters. The Henyey-Greenstein approximation was assumed for the scattering phase function [*Gasiewskii*, 1993]. The volumetric equivalent (effective) reflectivity factor Z_e can be related to the backscattering properties of the precipitation volume by means of

$$Z_e(r,\Omega_0) \equiv \frac{\lambda^4}{\pi^5|K|^2}\eta_e(r,\Omega_0) = \frac{\lambda^4}{\pi^5|K|^2}p(\Omega_s=\pi)k_s \tag{22}$$

where η_e is the volumetric equivalent radar reflectivity, $p(\Omega_s = \pi)$ is the volumetric scattering phase function computed in the backward direction (i.e., for the scattering solid angle Ω_s equal to π), and k_s is the volumetric scattering coefficient.

[34] The single-scattering (optical) parameter can now be illustrated using the precipitation profiles shown in Figure 2. As already said, the albedo at Ku and Ka bands can be significant for intense convection. Its high values should be indicators of the importance of multiple scattering effects, since the albedo weights the multiple scattering term in the radiative transfer equation (see (14)).

[35] Right panels of Figure 2 illustrate the volumetric albedo w as a function of the range (altitude). Roughly speaking, raindrops can be considered equally good radiometric absorbers and scatterers, while graupel particles are predominantly scatterers due to their ice composition and sizes (up to 3 mm in radius). At 14 GHz w is generally less than 0.85, reaching its maximum around heights between 4 and 8 km, where graupel scattering plays the major role. At 35 GHz w can be as high as 0.97 around the graupel concentration peaks.

[36] Left panels of Figure 3 show the same as in Figure 2, but for the one-way path attenuation A, which determines the attenuation factor L. Values of total path attenuation (i.e., from the surface to the antenna) of about 10 dB (20 dB for two-way path) are observed at 14 GHz for the heavy convection case, while at 35 GHz values of total A exceeds 35 dB (one way) even in the intense precipitation case. The impact of a two-way path attenuation being larger than 70 dB will reflect on the observed (attenuated) reflectivities and may preclude a practical measurement of rain rate near the surface at 35 GHz.

[37] In Figure 3 the right panels depict the vertical profiles of equivalent reflectivity factor Z_e at 14 and 35 GHz. High reflectivities (up to 49 dBZ) are obtained for the heavy rainfall profile, especially in the rain layers below the freezing level around 4.5 km and in the graupel layers between 5 and 8 km, and for the lowest frequency at 14 GHz. It is noted that Z_e decreases with the increase of frequency, that is with the decrease of wavelength.

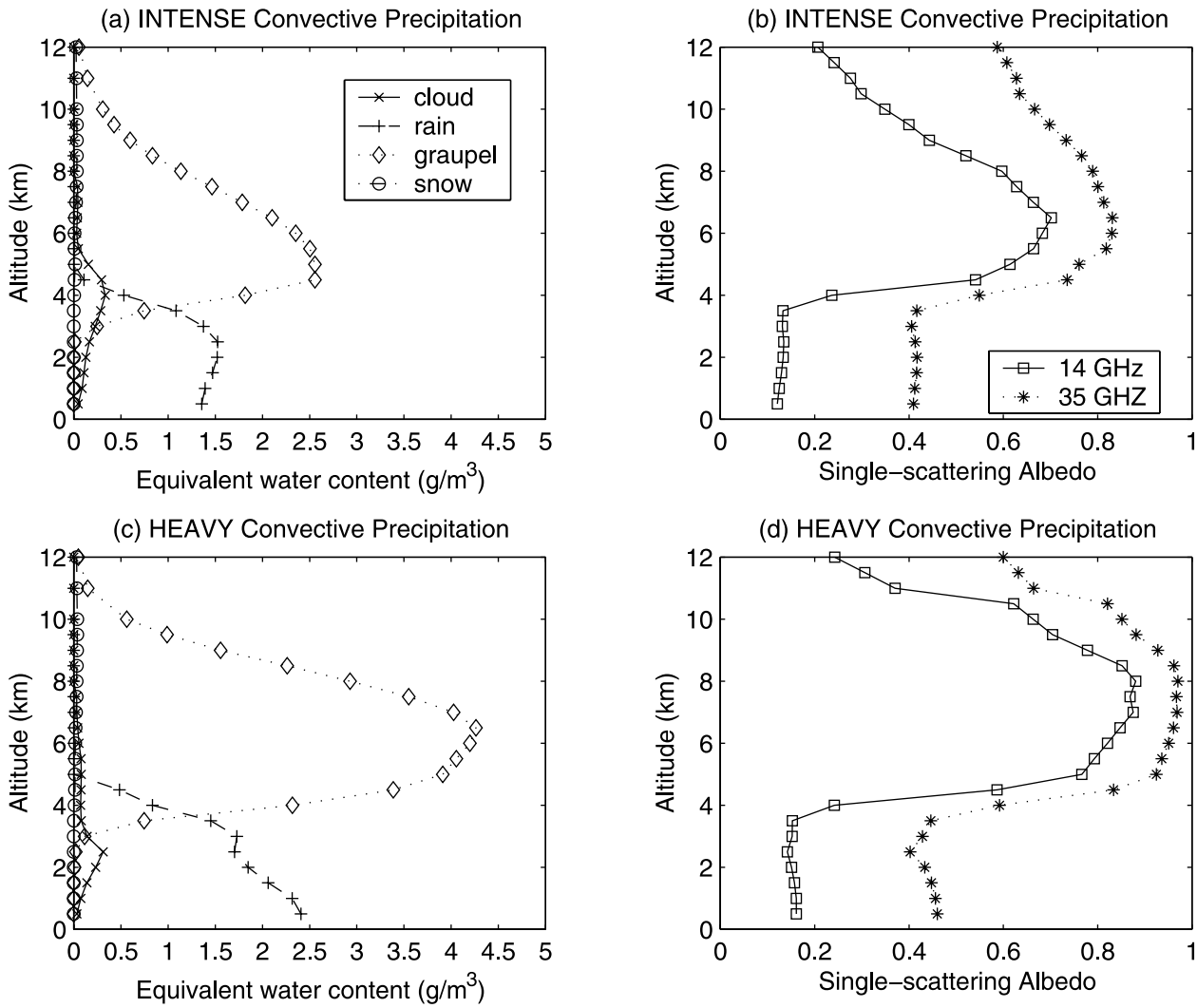

Figure 2. Panels (a) and (c): average vertical profiles of cloud, rain, graupel, and snow equivalent water contents for intense and heavy convective precipitation, shown in Figure 1. Panels (b) and (d): vertical profiles (nadir range) of single-scattering albedo at 13.8 and 35 GHz for intense and heavy precipitation.

[38] The obtained average profiles show, indeed, some peculiar characteristics of observed convective profiles. Strong updrafts and downdrafts are responsible for graupel generation and mixing around the zero-degree isotherm and above [*Tao et al.*, 1987]. Its vertical distribution, shown in Figure 2, is a key feature derived from mesoscale cloud-resolving models, otherwise not usually included in ad hoc rain structures [*Smith et al.*, 1992; *Yeh et al.*, 1995].

[39] Experimental evidence confirms that equivalent reflectivity Z_e of deep and highly convective clouds tends to remain constant or even increase above the freezing level in tropical mesoscale systems [*Szoke et al.*, 1986]. These observations are corroborated by airborne multiparameter data at Ku and Ka band in western Pacific where signatures of linear depolarization ratio and dual-frequency differential reflectivity clearly indicate the presence of high content of large-sized precipitating ice particles above the freezing level [*Kumagai and Meneghini*, 1993]. Consistently with Figure 2, one-way path attenuation measurements up to 10 dB were estimated from PR spaceborne measurements of convective clouds [*Iguchi et al.*, 2000], even though values up to 15 dB were retrieved from Ku-band airborne data [*Marecal et al.*, 1997; *Marzano et al.*, 1999a].

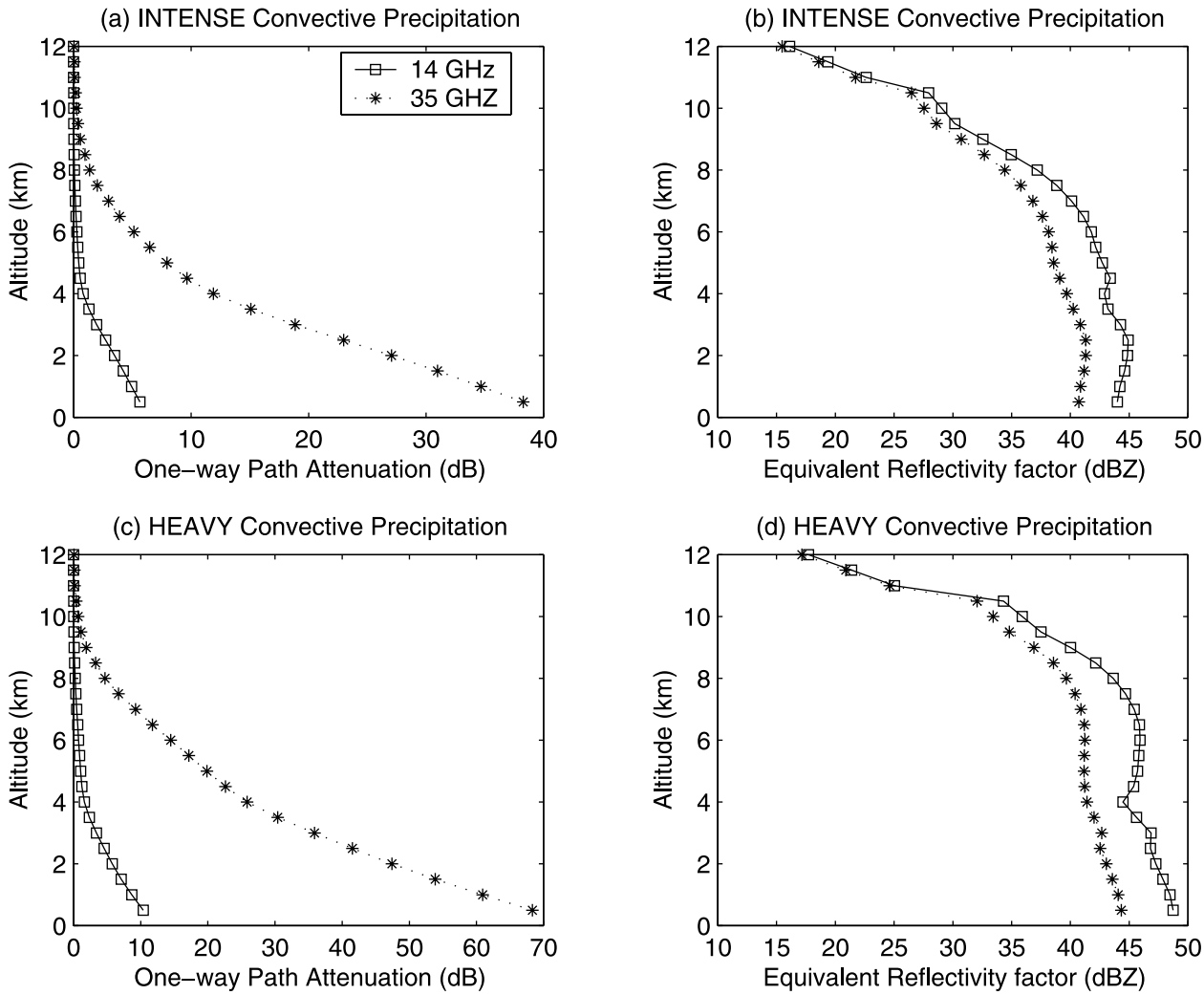

Figure 3. Panels (a) and (c): Vertical profiles (nadir range) of one-way path attenuation at 13.8 and 35 GHz for intense and heavy convective precipitation, shown in Figure 1. Panels (b) and (d): same, but for radar reflectivity factor at 13.8 and 35 GHz.

[40] Recent analyses of Lightning Image Sensor (LIS) aboard TRMM and collocated PR data have provided the opportunity to classify reflectivity profiles with respect to both convection (from PR) and lightning activity (from LIS) [*Dietrich et al.*, 2001]. Results have shown that Ku-band reflectivity profiles of convective clouds with significant lightning (greater than 1 flash per minute and square kilometer) denote Z_e peaks above 5 km, presumably due to ice particles. As a matter of fact, thunderstorm electrification is typically the result of colliding ice particles such that larger graupel particles (positively charged) tend to fall as opposed to lighter ice crystals (negatively charged) lifted to the upper cloud regions [*Solomon and Baker*, 1996]. The region, where the charge transfer takes place, is located approximately between -5 °C and -25 °C isotherm levels.

3.2. Simulation Results

[41] In this study the system noise temperature and the noise bandwidth of the receiver were not explicitly characterized. The minimum detectable reflectivity factor was taken to be 0 dBZ for graphical purposes, even though realistic values are above 10 dB to obtain an adequate reflectivity estimate. As a reference for the analysis of following results, assuming a rain slab of 4.5 km with a Marshall-Palmer drop size distribution in a Rayleigh regime and a signal-to-noise ratio (SNR) of 0

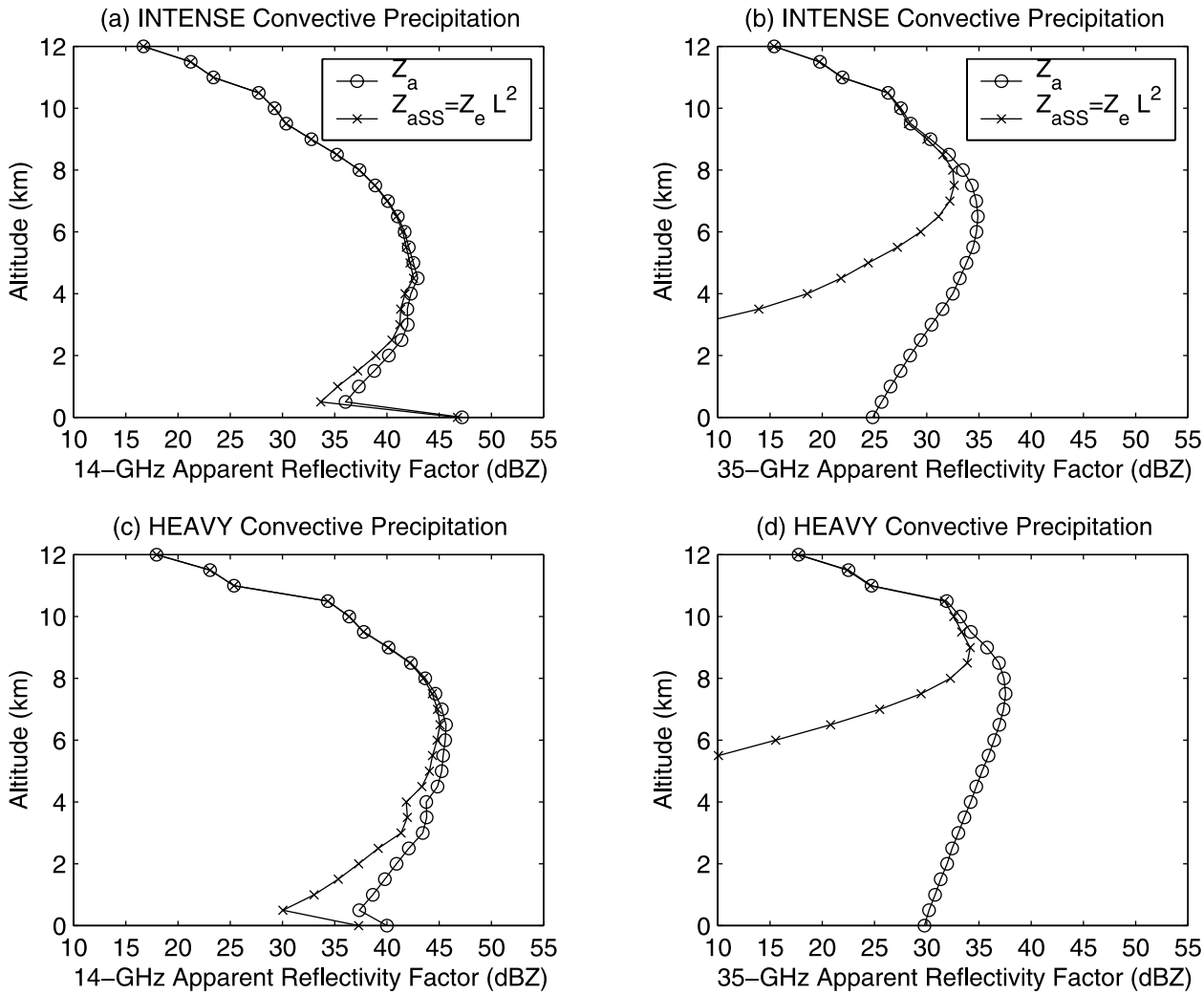

Figure 4. Panels (a) and (c): vertical profiles (nadir range) of apparent reflectivity factor Z_a (i.e., taking into account multiple scattering effects) and of single-scattering reflectivity factor Z_{aSS} (equal to Z_eL^2) at 13.8 GHz for intense and heavy convective precipitation, shown in Figure 1. Panels (b) and (d): same, but at 35 GHz.

dB, the theoretical dynamic ranges in the rain rate estimate are 0.15 to 90 mm/h at 14 GHz and 0.05 to 25 mm/h at 35 GHz [*Testud et al.*, 1992]. Previous minimum rain rate values are, indeed, higher in practice both for ground and space radars.

[42] A Lambertian model with a constant surface albedo of 0.1 was considered to describe the surface properties. The case of low surface albedo allows us to single out the atmospheric scattering effects and to simplify the Monte Carlo algorithm (see Section 2.2). This assumption is not too restrictive since the surface influence, for high frequencies and rain rates, is nearly negligible due to the predominance of precipitation scattering and absorption [*Marzano et al.*, 2000]. A collimated radar beam was supposed to be incident upon the top boundary of the cloud profiles in the nadir direction. It is worth mentioning that nadir viewing corresponds to the middle-swath along-track observation of PR.

[43] As demonstrated in Section 2, the apparent radar reflectivity can be evaluated from the received mean specific intensity, derived from (18) and (19). Figure 4 shows both the apparent reflectivity factor Z_a, taking into account both path attenuation and multiple scattering effects as from (8), and the single-scattering reflectivity factor Z_{aSS}, taking into account only single scattering and

path attenuation as from (11), at 14 and 35 GHz for the intense and heavy convective cases, as a function of the vertical range.

[44] At 14 GHz and for intense convection, Z_a and Z_{aSS} reflectivity profiles tend to coincide with a difference slightly increasing up to few dBZ's at 1 km altitude (see Figure 4a). At 35 GHz the surface influence is quickly masked by rain and graupel scattering as the frequency and heavy convection develops (see Figures 4b and 4d) and, correspondingly, the single scattering approximation becomes clearly inadequate for altitudes below the freezing level. At 14 GHz, for heavy convection, the difference between Z_a and Z_{aSS} becomes larger than 5 dBZ, while at 35 GHz (see Figures 4b and 4d) it is larger than 20 dBZ even around the freezing level. As the frequency increases, the altitude of the initial departure between Z_{aSS} and Z_a becomes higher and higher going from about 5 km (around the freezing level) at 14 GHz to about 9 km (around top height of graupel layers) at 35 GHz. This is explained by looking at the behaviors of respective albedo and path attenuation profiles in Figures 2 and 3.

[45] The difference between Z_a and Z_{aSS} gives a quantitative indication of the multiple scattering effects, while the difference between Z_{aSS} and Z_e provides a measure of path attenuation effects. As expected, for all the cases it holds $Z_{aSS} < Z_a < Z_e$. Previous figures prove that opposite effects are due to the combination of path attenuation and multiple scattering. On one hand, path attenuation is predominant for the single-scattering case and tends to reduce the equivalent reflectivity, especially at longer ranges from the radar. On the other hand, multiple scattering tends to increase the equivalent reflectivity, especially in the cloud regions characterized by large albedo, even though the effect of path attenuation still reduces its values with respect to the equivalent reflectivity ones.

[46] As usually done in the radar inverse problem, the profile of the rain rate R can be derived from a power relationship using an estimate of the equivalent reflectivity Z_e. Various Z_e-R have been proposed in literature, mainly depending on the storm type and operating frequency [*Sauvageot*, 1992]. A Z_e-R relation at 14 GHz has been here derived by choosing a rainfall terminal velocity consistent with the cloud-resolving model parameterization [*Tao et al.*, 1987; *Marzano and Bauer*, 2001]. Rain rate profiles have been then computed, given the rainwater content within each layer and its drop size distribution (see section 3.1). A nonlinear regression analysis of these simulations has finally provided a statistical Z_e-R relation, that is $Z_e = 110\ R^{1.6}$ with an error correlation (between estimates and true values) of about 0.9. Indeed, the goal of this exercise is to evaluate the impact of incoherent backscattering effects on rain rate profile retrieval in a simple way, disregarding all other possible error sources. Following results are substantially confirmed if other Z_e-R relationships are used as an inversion algorithm to retrieve R from radar observations [*Marzano et al.*, 2000].

[47] Left panels of Figure 5 give an example of the reconstructed rain rate profile for the intense and heavy convective cases, as a function of the vertical range. In order to compute R both the equivalent reflectivity factor Z_e and the apparent reflectivity factor Z_a divided by the path attenuation factor L, that is Z_a/L^2, were used. Notice that, if single scattering conditions hold, it should be $Z_{aSS}/L^2 \cong Z_e$. Rain rate values are shown only above 1 km in order to avoid the surface contamination.

[48] Using Z_a/L^2, the path attenuation correction does not necessarily provide a reconstruction of the "true" R profile, derived from Z_e, thus indicating the nonadequateness of single-scattering assumption especially for heavy convective rainfall [*Oguchi et al.*, 1994]. When using Z_a/L^2, an overestimation of the retrieved R in the high-albedo layers is evident below the freezing level. Looking at the differences in terms of R, the difference between the "true" rain rate value and that one derived from Z_a/L^2 is less than 10% percent for the intense convection and larger than 40% for the heavy convective profile.

3.3. Error Model

[49] Previous results suggest that, when dealing with heavy convective clouds, multiple scattering can be considered as a possible error source in the rain rate retrieval process. Inversion techniques, based on the classical radar equation given in (13), were developed for spaceborne radar observation in order to improve rain rate retrieval accuracy and reduce error impact [*Meneghini*, 1978; *Iguchi et al.*, 2000]. These errors were mainly attributed to, e.g., unrealistic Z_e-R and k-Z_e assumptions, radar calibration biases, nonuniform beam filling conditions, bright-band reflectivity contaminations. Constrained inversion methods might be still effectively applied if multiple scattering effects can be formally treated in the same way as errors are usually considered within these algorithms. This objective raises the issue to rewrite the generalized radar equation, given in (8), in a way formally equivalent to (13).

[50] In order to accomplish this task, it may be convenient to define the apparent specific attenuation (extinction coefficient) k_a as follows:

$$k_a(r) \equiv k(r) - k_{MS}(r) \tag{23}$$

where k_{MS} is the multiple-scattering specific attenuation defined as

$$k_{MS}(r) \equiv f_{MS} k(r) \equiv (1 - \varepsilon_a) k(r) \tag{24}$$

with f_{MS} being the multiple scattering factor. The latter is expressed in (24) by means of $\varepsilon_a = k_a(r)/k(r)$, denoted as

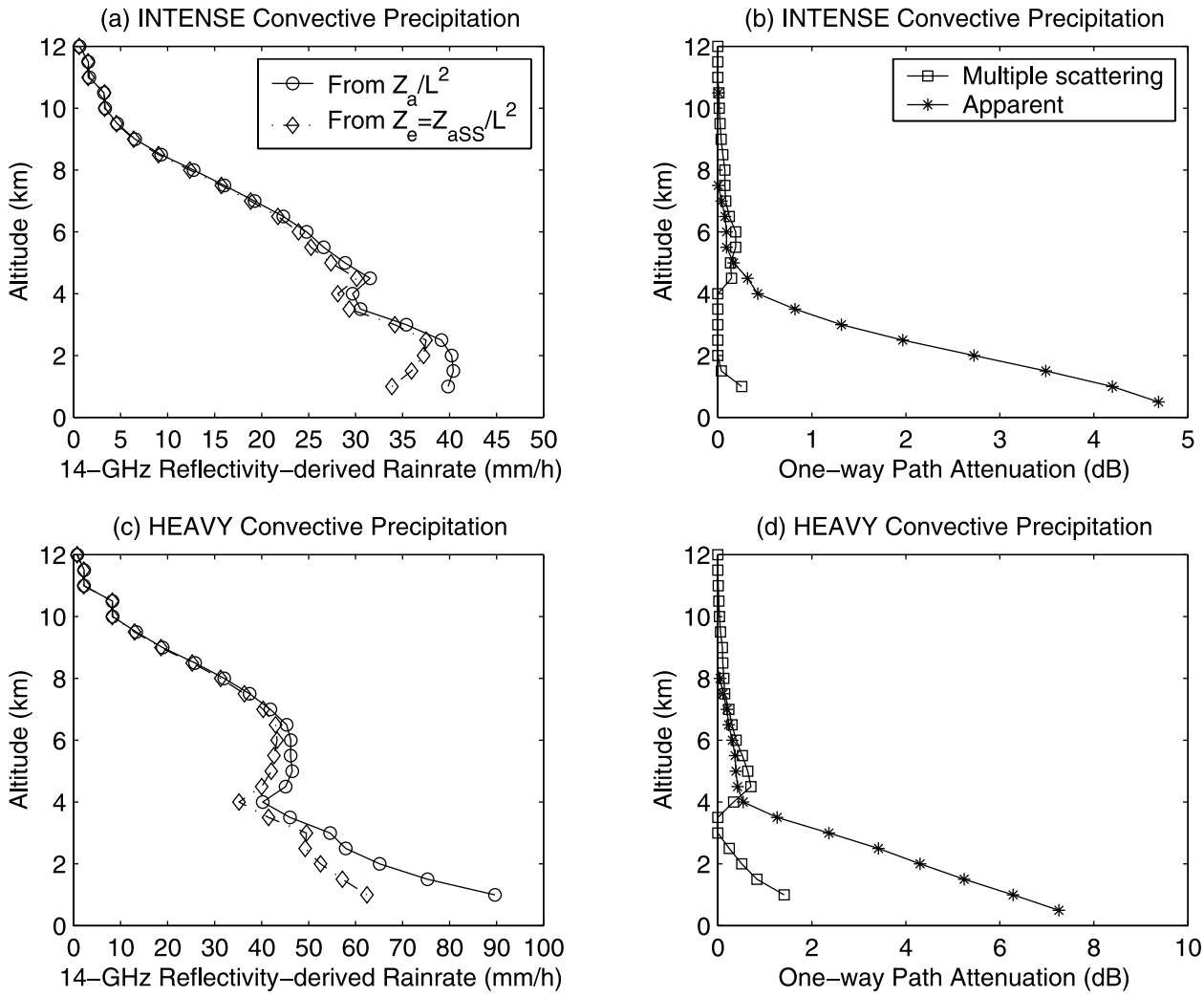

Figure 5. Panels (a) and (c): Vertical profiles (nadir range) of retrieved rain rate derived from the *Z-R* relation at 14 GHz using both the equivalent reflectivity factor (i.e., $Z = Z_e$) and the apparent reflectivity factor taking into account the two-way path-integrated attenuation (i.e., $Z = Z_a/L^2$) for intense and heavy convective precipitation, shown in Figure 1. Panels (b) and (d): vertical profiles (nadir range) of apparent path attenuation τ_a and multiple scattering path attenuation τ_{MS} at 13.8 GHz for intense and heavy convective precipitation, shown in Figure 1.

the apparent attenuation error. The definition of ε_a, to be used later on, is such that $\varepsilon_a \leq 1$ and, if multiple scattering effects are negligible, $f_{MS} = 0$ and $\varepsilon_a = 1$. From (12) and (23), the introduction of the apparent path attenuation τ_a is straightforward:

$$\tau_a(r) \equiv \int_0^r k_a(r')dr' = \int_0^r (1 - f_{MS})k(r')dr' = \tau(r) - \tau_{MS}(r) \quad (25)$$

where, consistently with (24), τ_{MS} is the multiple-scattering path attenuation.

[51] In view of these definitions, the apparent radar reflectivity factor Z_a in the generalized radar equation given in (8), can be formally expressed as follows:

$$Z_a(r, \Omega_0) \equiv Z_e(r, \Omega_0)e^{-2\tau_a(r)} = Z_e(r, \Omega_0)L_a^2(r) \quad (26)$$

that is, by substituting (25),

$$Z_a(r, \Omega_0) \equiv Z_e(r, \Omega_0)e^{2\tau_{MS}(r)}e^{-2\tau(r)} \quad (27)$$

where L_a is the one-way apparent path attenuation factor. By definition, it holds that $L_a(r) \leq L(r)$. Note again that, in case of negligibility of incoherent effects, $\tau_{MS} = 0$ and $Z_a = Z_{aSS}$ as expected. Finally, from (27) we can derive the multiple scattering path attenuation τ_{MS} as a function of apparent and equivalent reflectivity factors:

$$\tau_{MS}(r) = \tau(r) + ln\left[\frac{Z_a(r,\Omega_0)}{Z_e(r,\Omega_0)}\right]^{1/2} \tag{28}$$

[52] The latter expression can be quantified since on the right side all terms were already computed during the numerical simulation illustrated in the previous section. The result is shown in the right panels of Figure 5 where the range behavior of τ_{MS} (expressed in dB) at 14 GHz is plotted together with the apparent attenuation τ_a (expressed in dB) for both the intense and heavy cloud convective profiles. Multiple scattering attenuation is pronounced at longer range (near the surface) and where ice graupel is present (between 4 and 8 km). It is less than 1 dB for intense convection, but can reach up to 2 dB within the near-surface rain layer for heavy convection.

[53] The possible role of the uncertainty due to this incoherent effect within single-frequency radar inversion techniques can be now approached. Figure 5 has shown that potential errors in the rain rate retrieval for heavy convection cases can be as high as 50%. Indeed, spaceborne radar retrieval algorithms generally exploit auxiliary measurements used as constraints within the inversion procedure [*Iguchi et al.*, 2000]. The question is whether these techniques can be still successfully applied to reduce the uncertainties due to multiple scattering in convective clouds.

[54] To deepen this issue, let us rewrite the generalized radar equation, given in (26), as follows:

$$Z_a(r,\Omega_0) = Z_e(r,\Omega_0)e^{-2\int_0^r k_a(r')dr'} \tag{29}$$

where the objective is to estimate Z_e given the measured Z_a. In order to accomplish the error analysis and to solve the inverse problem, a general statistical k-Z_e relation can be assumed [*Iguchi and Meneghini*, 1994]:

$$k(r) = \alpha(r)[Z_e(r,\Omega_0)]^{\beta} \tag{30}$$

with α and β coefficients depending on frequency, precipitation type and hydrometeor composition [*Sauvageot*, 1992]. If $\varepsilon_a = 1$ and (30) is substituted in (29), the classical Hitschfeld-Bordan solution can be derived [*Meneghini*, 1978]. As known, this solution results to be highly unstable especially in strong path-attenuation conditions. If $\varepsilon_a < 1$, k_a is unknown since k_{MS} is unknown. However, we can interpret k_a as a perturbation (error) of k through the apparent attenuation error ε_a. From (24) and (30) we get

$$k_a(r) = \varepsilon_a\alpha(r)[Z_e(r,\Omega_0)]^{\beta} \tag{31}$$

[55] Indeed, the previous equation together with (29) can be solved by applying the so-called α-adjustment method which resort to the surface reference technique (SRT) to impose a total (radar-to-surface) path attenuation measurement as a constraint [*Iguchi and Meneghini*, 1994]. The α-adjustment solution is given by

$$\hat{Z}_e(r,\Omega_0) = \frac{Z_a(r,\Omega_0)}{[1-\varepsilon_a\beta S(r)]^{1/\beta}} \tag{32}$$

with the integral S expressed as

$$S(r) = \int_0^r 2\alpha(r')[Z_a(r,\Omega_0)]^{\beta}dr' \tag{33}$$

and the apparent attenuation error ε_a derived from

$$\varepsilon_a = \frac{1-[L_a(r_s)]^{2\beta}}{\beta S(r_s)} = \frac{\tau_a(r_s)}{\tau(r_s)} \tag{34}$$

being r_s the radar range of the surface (see Figure 1). It is worth mentioning that, from previous results, the SRT method may be used at 14 GHz, but not at 35 GHz where any practical radar will never see the surface for intense or heavy rains.

[56] If the assumed k-Z_e relation is accurate enough for all ranges and other uncertainty effects (such as the nonuniform beam filling and radar calibration bias) can be assumed negligible, an evaluation of $L_a(r_s)$ allows to derive ε_a and, thus, to retrieve Z_e. As mentioned, the surface reference technique can give such an estimate by means of

$$\hat{L}_a(r_s) = \left[\frac{Z_a(r_s)}{Z_e(r_s)}\right]^{1/2} \tag{35}$$

where $Z_e(r_s)$ is derived in nonrainy conditions under surface stationary conditions.

[57] When (34) or (35) are applied to the considered numerical simulation (see Figures 4 and 5), it results that $\varepsilon_a = 0.94$ and $\varepsilon_a = 0.83$ for the intense and heavy convective profiles, respectively. These values of ε_a are consistent with the histograms of the attenuation correction factor ε of convective rain over land, derived from PR measured data [*Iguchi et al.*, 2000]. If other error sources are present, ε will be of course higher or lower than ε_a depending on the error type.

[58] Thus, we can conclude that, even though the multiple scattering impact in convective clouds is diffi-

cult to be isolated, it can be treated as an error source affecting the estimate of specific attenuation k. A suitable constrained inversion technique, such as the α-adjustment method, can be applied to reduce, and possibly correct for, the effects of multiple scattering.

4. Summary and Conclusions

[59] The deduction of a generalized radar equation was carried out from the definition of the apparent radar reflectivity, thus including the multiple scattering phenomenon in its formulation. A probabilistic form of the apparent radar reflectivity was derived within the theoretical context of the radiative transfer theory. It was demonstrated that, if single scattering conditions hold, the generalized radar equation reduces to the classical radar equation.

[60] In order to apply the previous concepts, precipitation profiles were extracted from a microphysical cloud-resolving model, simulating an intense squall line. In order to classify the results, the hydrometeor vertical profiles were grouped in two categories of intense and heavy convective rainfall, represented by average profiles. The optical parameters, such as equivalent reflectivity, path attenuation, and albedo, of the precipitating cloud profiles were discussed pointing out the dominant impact of graupel particles at the considered frequencies. Measurements of convective clouds, available in literature, were used to ascertain the realistic appearance of the obtained synthetic cloud profiles.

[61] Numerical results of nadir-looking radar observations showed that the difference between multiple-scattering reflectivity factor Z_a and the single-scattering one Z_{aSS} can give an indication of the multiple scattering effects, while the difference between Z_{aSS} and the equivalent reflectivity factor Z_e provides a measure of the path attenuation effects, holding for all the cases $Z_{aSS} < Z_a < Z_e$. Opposite effects are due to the combination of path attenuation and multiple scattering. While on one hand, path attenuation is the predominant contribution for the single-scattering case and tends to reduce the equivalent reflectivity, on the other hand, multiple scattering tends to increase the single-scattering reflectivity, especially in the cloud regions characterized by large albedo. These incoherent effects are significantly appreciable at 14 GHz for heavy convection and at 35 GHz even for intense convection.

[62] Spaceborne radar observations of precipitation profiles were simulated by means of a radiative transfer model, using a Monte Carlo solution technique. The effects of precipitation multiple scattering were evaluated at two attenuating frequencies and for nadir observations. The PR 13.8-GHz frequency band was chosen together with the channels at 35 GHz. The choice of the latter frequencies reflects the emerging interest on the use of a dual-frequency radar, to be placed aboard the future TRMM follow-on platform [*Mugnai et al.*, 2002].

[63] When converting reflectivity in rain rate profiles through a Z_e-R relation at 14 GHz, the difference between "true" R value and that one derived from attenuation-corrected apparent reflectivity (i.e., Z_a/L^2) can be about 10% for intense and about 40% for heavy convective profiles. Even though the multiple scattering impact is difficult to be identified, it was shown it can be treated as an error source affecting the estimate of specific attenuation k. A suitable constrained inversion techniques, such as the α-adjustment method, can be then applied to reduce, and possibly correct, for the effects of multiple scattering themselves. In real conditions, these incoherent effects will be superimposed to other error sources so that their verification remains a cumbersome open problem. Indeed, laboratory measurements tend to confirm the significance of multiple scattering effects on the radar response at microwave band [*Oguchi et al.*, 1998].

[64] **Acknowledgments** This work was partially supported by the Italian Space Agency (ASI), the Italian Ministry of Education and University (MIUR) and by the European Union (EU) through the Euro-TRMM project. The authors would like to thank Dr. Kummerow and Dr. Tao from NASA Goddard Space Flight Center (Greenbelt, Maryland) for making the cloud model outputs available. Reviewers' suggestions are gratefully acknowledged.

References

Bringi, V. N., A. Hendry, Technology of polarization diversity radar in meteorology, in *Radar Meteorology*, edited by D. Atlas, pp. 153–190, Am. Meteorol. Soc., Boston, Mass., 1990.

Collins, D. G., W. G. Blattner, M. B. Walls, and H. G. Horak, Backward Mon Carlo calculations of the polarization characteristics of the radiation emerging from a spherical-shell atmospheres, *Appl. Opt.*, *32*, 2684–2696, 1972.

Dietrich, S., R. Solomon, C. Adamo, A. Mugnai, Rainfall monitoring at geostationary scale: Potential of lightning data in a rapid update approach, paper presented at Meteorological Satellite Data Users' Conference, Eur. Org. for the Exploit. of Meteorol. Satell., Antalya, Turkey, 1–5 Oct. 2001.

Fujita, M., An algorithm for estimating rain rate by a dual-frequency radar, *Radio Sci.*, *18*, 697–708, 1983.

Gasiewskii, A. J., Microwave radiative transfer in hydrometeors, in *Atmospheric Remote Sensing by Microwave Radiometry*, edited by M. A. Jansen, pp. 91–144, John Wiley, New York, 1993.

Haddad, Z., E. Im, and S. L. Durden, Optimal estimation of rain-rate profiles from single-frequency radar echoes, *J. Appl. Meteorol.*, *35*, 214–228, 1996.

Iguchi, T., and R. Meneghini, Intercomparison of single-frequency methods for retrieving a vertical rain profile from airborne or spaceborne radar data, *J. Atmos. Oceanic Technol.*, *11*, 1507–1516, 1994.

Iguchi, T., T. Kozu, R. Meneghini, J. Awaka, and K. Okamoto, Rain-profiling algorithm for the TRMM precipitation radar, *J. Appl. Meteorol.*, *39*, 2038–2052, 2000.

Ishimaru, A., *Wave Propagation and Scattering in Random Media*, vols. *1 and 2*, Academic, San Diego, Calif., 1978.

Ishimaru, A., R. Woo, J. W. Armstrong, and D. C. Blackman, Multiple scattering calculations of rain effects, *Radio Sci.*, *17*, 1425–1433, 1982.

Ito, S., T. Oguchi, T. Iguchi, H. Kumagai, and R. Meneghini, Depolarization of radar signals due to multiple scattering in rain, *IEEE Trans. Geosci. Remote Sens.*, *33*, 1057–1062, 1995.

Kumagai, H., and R. Meneghini, Preliminary results from multiparameter airborne rain radar measurement in the Western Pacific, *J. Appl. Meteorol.*, *32*, 4431–4440, 1993.

Kummerow, C., W. Barnes, T. Kozu, J. Shiue, and J. Simpson, The Tropical Rainfall Measuring Mission (TRMM) sensor package, *J. Atmos. Oceanic Technol.*, *15*, 809–817, 1998.

Lin, Y. C., and K. Sarabandi, A Monte Carlo coherent scattering model for forest canopies using fractal-generated tress, *IEEE Trans. Geosci. Remote Sens.*, *37*, 440–451, 1999.

Marecal, V., T. Tani, P. Amayenc, C. Klapisz, E. Obligis, and N. Viltard, Rain relations inferred from microphysical data in TOGA-COARE and their use to test a rain-profiling method from radar measurements at Ku-band, *J. Appl. Meteorol.*, *36*, 1629–1646, 1997.

Marzano, F. S., and P. Bauer, Sensitivity analysis of airborne microwave retrieval of stratiform precipitation to the melting layer parameterization, *IEEE Trans. Geosci. Remote Sen.*, *39*, 75–91, 2001.

Marzano, F. S., A. Mugnai, E. A. Smith, X. Xiang, J. Turk, and J. Vivekanandan, Active and passive remote sensing of precipitating storms during CaPE, part II, Intercomparison of precipitation retrievals from AMPR radiometer and CP-2 radar, *Meteorol. Atmos. Phys.*, *54*, 29–51, 1994.

Marzano, F. S., A. Mugnai, G. Panegrossi, N. Pierdicca, E. A. Smith, and J. Turk, Bayesian estimation of precipitating cloud parameters from combined measurements of spaceborne microwave radiometer and radar, *IEEE Trans. Geosci. Remote Sens.*, *37*, 596–613, 1999a.

Marzano, F. S., E. Fionda, and P. Ciotti, Simulation of radiometric and attenuation measurements along Earth-satellite links in the 10- to 50-GHz band through horizontally finite convective raincells, *Radio Sci.*, *34*, 841–858, 1999b.

Marzano, F. S., L. Roberti, and A. Mugnai, Impact of incoherent backscattering upon radar echoes above 10 GHz, *J. Phys. Chem. Earth B*, *25*(10), 300–305, 2000.

Marzoug, M., and P. Amayenc, Improved range-profiling algorithm of rainfall rate from a spaceborne radar with path-integrated attenuation constraint, *IEEE Trans. Geosci. Remote Sens.*, *29*, 584–592, 1991.

Marzoug, M., and P. Amayenc, A class of single and dual frequency algorithms for rain-rate profiling from a spaceborne radar, part I, Principle and tests from numerical simulations, *J. Atmos. Oceanic Technol.*, *11*, 1480–1506, 1994.

Meneghini, R., Rain rates estimates for an attenuating radar, *Radio Sci.*, *13*, 459–470, 1978.

Meneghini, R., K. Nakamura, W. Ulbrich, and D. Atlas, Experimental tests of methods for the measurement of rainfall rate using an airborne dual-wavelength radar, *J. Atmos. Oceanic Technol.*, *6*, 637–651, 1989.

Morel, A., and B. Gentili, Diffuse reflectance of oceanic waters: Its dependence on sun angle as influence by the molecular scattering contribution, *Appl. Opt.*, *30*, 4427–4438, 1991.

Mugnai, A., et al., Potential improvement of rainfall estimation from the Global Precipitation Mission, in *Proceedings of the 2nd European Geophysical Society Plinius Conference on Mediterranian Storms, Siena (Italy), 16–18 October 2000*, edited by A. Mugnai, F. Guzzetti, and G. Roth, pp. 91–108, Eur. Geophys. Soc., Katlenburg-Lindau, Germany, 2002.

Oguchi, T., N. Ishida, and T. Ihara, Effect of multiple scattering on the estimation of rainfall rates using a dual wavelenght radar techniques, *IEEE Trans. Geosci. Remote Sens.*, *32*, 943–946, 1994.

Oguchi, T., S. Ishii, S. Ito, and T. Manabe, Laboratory measurements of radar depolarization signatures in microwave pulse transmission through randomly distributed spherical scatterers, *IEEE Trans. Geosci. Remote Sens.*, *36*, 1011–1015, 1998.

Olson, W. S., C. D. Kummerow, G. M. Heymsfield, and L. Giglio, A method for combined passive-active microwave retrievals of cloud and precipitation parameters, *J. Appl. Meteorol.*, *35*, 1763–1789, 1996.

Roberti, L., Monte Carlo radiative transfer in the microwave and in the visible: Biasing techniques, *Appl. Opt.*, *36*, 7929–7938, 1997.

Roberti, L., J. Haferman, and C. D. Kummerow, Microwave radiative transfer through horizontally inhomogeneous precipitating clouds, *J. Geophys. Res.*, *99*, 16,707–16,718, 1994.

Sauvageot, H., *Radar Meteorology*, Artech House, Norwood, Mass., 1992.

Smith, E. A., A. Mugnai, H. J. Cooper, G. J. Tripoli, and X. Xiang, Foundations for statistical-physical precipitation retrieval from passive microwave satellite measurements, part I, Brightness-temperature properties of a time-dependent cloud-radiation model, *J. Appl. Meteorol.*, *31*, 506–531, 1992.

Solomon, R., and M. B. Baker, A one-dimensional lightning parameterization, *J. Geophys. Res.*, *101*, 14,983–14,990, 1996.

Szoke, E. J., E. J. Zipser, and D. P. Jorgenson, A radar study of convective cells in mesoscale systems in GATE, part I, Ver-

tical profile statistics and comparison with hurricanes, *J. Atmos. Sci.*, *43*, 182–197, 1986.

Tao, K., J. Simpson, and S. T. Soong, Statistical properties of a cloud ensemble: A numerical study, *J. Atmos. Sci.*, *44*, 3175–3187, 1987.

Testud, J., P. Amayenc, and M. Marzoug, Rainfall-rate retrieval from a spaceborne radar: Comparison between single-frequency, dual-frequency and dual-beam techniques, *J. Atmos. Oceanic Technol.*, *9*, 599–623, 1992.

Tsang, L., J. A. Kong, R. T. Shin, *Theory of Microwave Remote Sensing*, John Wiley, New York, 1985.

Weinman, J. A., R. Meneghini, and K. Nakamura, Retrieval of precipitation profiles from airborne radar and passive radiometer measurements: Comparison with dual-frequency radar measurements, *J. Appl. Meteorol.*, *29*, 981–993, 1990.

Yeh, H. Y. M., N. Prasad, R. Meneghini, J. A. Jones, and R. F. Adler, Cloud model-based simulation of spaceborne radar observations, *J. Appl. Meteorol.*, *34*, 175–197, 1995.

S. Di Michele, A. Mugnai, and A. Tassa, Istituto di Scienze dell'Atmosfera e del Clima (ISAO), Consiglio Nazionale delle Ricerche (CNR), Via Fosso del Cavaliere, 100-00133 Roma, Italy.

F. S. Marzano, Dipartimento di Ingegneria Elettrica, Centro di Eccellenza CETEMPS, Università dell'Aquila, Monteluco di Roio, 67040L'Aquila, Italy. (marzano@ing.univaq.it)

L. Roberti, BTexact Technologies, Adastral Park, Martlesham Heath, Ipswich IP5 3RE, UK.